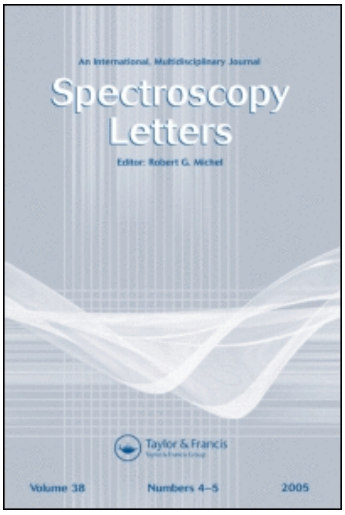

Spectroscopy Letters
Publication details, including instructions for authors and subscription information:
http://www.informaworld.com/smpp/title~content=t713597299

Excitation and Emission Spectra of $Cs_2NaLnCl_6$ Crystals Using Synchrotron Radiation

Peter A. Tanner[a]; Chang-Kui Duan[ab]; Bing-Ming Cheng[c]
[a] Department of Biology and Chemistry, City University of Hong Kong, Kowloon, Hong Kong S.A.R., Peoples' Republic of China [b] Institute of Modern Physics, Chongqing University of Post and Telecommunications, Chongqing, Peoples' Republic of China [c] National Synchrotron Radiation Research Center, Hsinchu, Taiwan

Online publication date: 30 July 2010

To cite this Article Tanner, Peter A. , Duan, Chang-Kui and Cheng, Bing-Ming(2010) 'Excitation and Emission Spectra of $Cs_2NaLnCl_6$ Crystals Using Synchrotron Radiation', Spectroscopy Letters, 43: 5, 431 — 445
To link to this Article: DOI: 10.1080/00387010.2010.505856
URL: http://dx.doi.org/10.1080/00387010.2010.505856

Spectroscopy Letters, 43:431–445, 2010

ISSN: 0038-7010 print/1532-2289 online
DOI: 10.1080/00387010.2010.505856

Taylor & Francis
Taylor & Francis Group

Excitation and Emission Spectra of $Cs_2NaLnCl_6$ Crystals Using Synchrotron Radiation

Peter A. Tanner[1], Chang-Kui Duan[1,2], and Bing-Ming Cheng[3]

[1]Department of Biology and Chemistry, City University of Hong Kong, Kowloon, Hong Kong S.A.R., Peoples' Republic of China
[2]Institute of Modern Physics, Chongqing University of Post and Telecommunications, Chongqing, Peoples' Republic of China
[3]National Synchrotron Radiation Research Center, Hsinchu, Taiwan

ABSTRACT The visible emission and vacuum ultraviolet excitation spectra of the series $Cs_2NaLnCl_6$ (Ln = Y, Nd, Sm, Eu, Tb, Er, Yb) and Cs_2NaYCl_6:Ln^{3+} (Ln = Sm, Er) have been recorded using synchrotron radiation at room temperature, and in some cases at 10 K. The excitation spectra comprise features associated with charge transfer, excitation from the valence to conduction band, and impurity bands. No d–f emissions were observed for these Ln^{3+} ions, so that the emission bands comprise intraconfigurational $4f^N$–$4f^N$ transitions and impurity bands, whose natures are discussed. Theoretical simulations of the f–d absorption spectra have been included. The comparison with data from the synchrotron at Desy enables a comprehensive account of the ground (or vibrationally excited ground for Ln^{2+}) states of the Ln^{3+} $4f^N$, Ln^{3+} $4f^{N-1}5d$, and Ln^{2+} $4f^{N+1}$ configurations relative to the valence and conduction bands of $Cs_2NaLnCl_6$, for which the band gaps are between 6.6 and 8.1 eV.

KEYWORDS 4f–5d spectra, charge transfer, energy levels, excitation spectra, lanthanide ion, spectral intensities

INTRODUCTION

Since the $4f^N$ energy levels of lanthanide ions have been well investigated and characterized,[1] current interest resides in the higher energy electronic configurations, notably $4f^{N-1}5d$. This configuration has been extensively studied for high band-gap fluoride hosts, and detailed simulations of the excitation spectra have been presented.[2–5] Fewer studies of the $4f^{N-1}5d$ configuration are available for low-band gap hosts, with the exception of oxides.[6–9] We have given a preliminary account of the synchrotron excitation and emission spectra of tripositive lanthanide ions—Ln = Ce, Eu, Gd, Er, Tm, Yb—in hexachloroelpasolite hosts using the synchrotron at Desy, Hamburg.[10] In this case, most of the $4f^N \rightarrow 4f^{N-1}5d$ transitions reside above the host band gaps, which are in the region of 7.4 ± 0.8 eV. Many features were observed that were not readily explained or that were attributed to impurities due to the deliquescent nature of the crystals. A more complete reinvestigation is presented herein, including both neat

Received 21 September 2009; accepted 22 October 2009.

Address correspondence to Peter A. Tanner, Department of Biology and Chemistry, City University of Hong Kong, Tot Chee Avenue, Kowloon, Hong Kong S.A.R., P.R. China. E-mail: bhtan@cityu.edu.hk

and doped crystals, using the synchrotron at Hsinchu, Taiwan, Japan, which includes the tripositive ions Y, Nd, Sm, Eu, Tb, Er, and Yb. This has enabled a comprehensive and systematic interpretation of the excitation spectra to be achieved, together with a unified parameter set for the calculation of $4f^{N-1}5d$ energy levels and presentation of simulated $4f^N \rightarrow 4f^{N-1}5d$ spectra. We envisage that this data will serve as a reference for future excited-state absorption experiments for these systems.

The series $Cs_2NaLnCl_6$ comprises ideal hosts for lanthanide ions because the octahedral (O_h) site symmetry of the $LnCl_6^{3-}$ moiety conveys high energy level degeneracies and strict transition selection rules. The low phonon energies (in most cases below 300 cm^{-1}) enable radiative processes to dominate so that there are many luminescent levels for these systems.

MATERIALS AND METHODS

General

The synthesis of polycrystalline samples of $Cs_2NaLnCl_6$ and Cs_2NaYCl_6:Ln^{3+} by Morss Method C and subsequent passage of the powders in vacuum in quartz tubes through a Bridgman furnace have been described elsewhere.[11] The precursors were Ln_2O_3 (Strem Chemicals and International Laboratory) of 99.99% or 99.999% purity. The measurement of the vacuum ultraviolet spectrum at NSRRC has been previously described.[12] Briefly, vacuum ultraviolet (VUV) radiation was dispersed with a high-flux cylindrical grating monochromator, of focal length 6 m, and beam line.[13] The intensity of the VUV light was monitored through light reflected from a LiF beam splitter placed before the phosphor and at 45° from the beam line. A small fraction of the reflected light beam passed one additional LiF plate and impinged on a glass window coated with sodium salicylate. The luminescent signal subsequently detected with a photomultiplier tube in a photon-counting mode was employed for normalization. The light transmitted through the LiF beam splitter irradiated a sample, which was aligned at about 40–50° with respect to both the incident VUV source and the entrance slit of the emission monochromator. The irregularly shaped crystal was mounted in a sample holder attached to a rotatable XYZ stage. The monochromator to disperse luminescence had a focal length of 0.32 m and a grating of 1200 grooves mm^{-1} blazed at 500 nm; with reciprocal linear dispersion of 2.5 nm mm^{-1}. The scanning of this monochromator was controlled with a spectral-link module, which was in turn controlled with a PC via a RS232 interface. The luminescent intensity of the hexachloroelpasolite was detected by a photomultiplier in the photon-counting mode.

For clarity of presentation, the emission spectra are presented with a linear wavelength scale, whereas the scale is linear in energy (cm^{-1}) for the excitation spectra.

Theory

Although the method of calculation of $4f^N$ and $4f^{N-1}5d$ energy levels has been presented in detail elsewhere, for the sake of completeness, it is briefly introduced here. The standard phenomenological crystal-field Hamiltonian $H(4f)$ and its extension[2,14] were employed:

$$H = H(4f) + H(5d) + H_{int}(4f, 5d), \qquad (1)$$

where $H(4f)$, $H(5d)$, and $H_{int}(4f,5d)$ describe the interactions experienced by or between the 4f electrons; the interactions experienced by the 5d electron; and the interaction between 4f and 5d electrons, respectively, as shown below:

$$\begin{aligned} H(4f) = {} & E_{avg} + \sum_{k=2,4,6} F^k \mathbf{f}_k(f) + \zeta_{4f} \mathbf{s}_{4f} \cdot \mathbf{l}_{4f} \\ & + \sum_{i=2-4,6-8} T^i \mathbf{t}_i(f) + \alpha \mathbf{L}^2(f) \\ & + \beta \mathbf{G}(G_2(f)) + \gamma \mathbf{G}(G_7(f)) \\ & + \sum_{k=0,2,4} M^k \mathbf{m}_k(f) + \sum_{k=2,4,6} P^k \mathbf{p}_k(f) \\ & + \sum_{kq} B_q^k \mathbf{C}_q^{(k)}(f); \end{aligned} \qquad (2)$$

$$H(5d) = \zeta_{5d} \mathbf{s}_{5d} \cdot \mathbf{l}_{5d} + \sum_{kq} B_q^k(d) \mathbf{C}_q^{(k)}(d);$$

$$\begin{aligned} H_{int}(4f, 5d) = {} & E_{exc} + \sum_{k=2,4} F^k(fd) \mathbf{f}_k(fd) \\ & + \sum_{k=1,3,5} G^k(fd) \mathbf{g}_k(fd). \end{aligned}$$

Here the italic and bold letters represent parameters and operators, respectively, and (f), (d), and (fd) are used to show that the operators are interactions for 4f electrons, interactions for the 5d electron, and

interactions between 4f and 5d electrons, respectively. The parameter E_{avg} in $H(4f)$ serves to shift all the levels so that the energy of the lowest level of $4f^N$ is zero; the second and third terms in $H(4f)$ are the two strongest interactions for the $4f^N$ configuration ($4f^{N-1}$ core), i.e., the Coulomb and spin-orbit interactions; the last term in $H(4f)$ is the crystal-field interaction experienced by 4f electrons, which can be described by the two parameters B_4 for the operator $C_0^{(4)}(4f) + \sqrt{5/14}[C_{-4}^{(4)}(4f) + C_4^{(4)}(4f)]$ and B_6 for the operator $C_0^{(6)}(4f) - \sqrt{7/2}\ [C_{-4}^{(6)}(4f) + C_4^{(6)}(4f)]$; and the other terms are effective interactions to describe various effects due to configuration interaction. The two terms in $H(5d)$ are the spin-orbit interaction and the strong crystal-field interaction, $B_4(d)$, $\left\{C_0^{(4)}(5d) + \sqrt{5/14}[C_{-4}^{(4)}(5d) + C_4^{(4)}(5d)]\right\}$ experienced by the 5d electron. The $H_{int}(4f,5d)$ parameter E_{exc} describes the separation between the barycenters of the $4f^N$ and $4f^{N-1}5d$ levels; and the second and third terms are the direct and exchange Coulomb interaction between 4f and 5d electrons.

Table 1 lists the parameters employed in the energy-level calculations. The parameters for $4f^N$ configuration were available from the literature, with those for Ce^{3+} refitted herein from data in Ref. [11]; Pr^{3+} from Ref. [15]; Nd^{3+}[16] Sm^{3+}[17] Eu^{3+} and Gd^{3+}[18] Tb^{3+} refitted from data in Ref. [19]; Er^{3+}[20] Tm^{3+}[21] and Yb^{3+}.[22] The parameters M^2, M^4, P^4, and P^6 are not listed in Table 1 since they are fixed by the ratios $M^2/M^0 = 0.56$; $M^4/M^0 = 0.31$; $P^4/P^2 = 0.5$; and $P^6/P^2 = 0.1$. The F^k parameters for $4f^{N-1}5d$ were scaled from the values for $4f^N$ by the corresponding ratio of calculated F^k values[23] for each k. The parameter describing the spin-orbit interaction of 4f electrons was determined in the same way. The parameters $F^2(fd)$, $F^4(fd)$, and $G^1(fd)$, $G^3(fd)$, and $G^5(fd)$ describing the Coulomb interactions between 4f and 5d electrons were scaled from the *ab initio* value[23] by the factor $\eta_{fd} = 0.53$, which

TABLE 1 Parameter Values (cm^{-1}) Used in the Simulation of f–d Absorption Spectra

Ion	Ce^{3+}	Pr^{3+}	Nd^{3+}	Sm^{3+}	Eu^{3+}	Gd^{3+}	Tb^{3+}	Er^{3+}	Tm^{3+}	Yb^{3+}
$4f^N$: N=	1	2	3	5	6	7	8	11	12	13
F^2		67325	71106	78165	83902	78686	88320	96717	99725	
F^4		49539	51440	56612	59990	70120	62925	67374	68592	
F^6		32258	35068	40172	41364	43596	45088	47541	48231	
ζ	624	756	880	1166	1324	1505	1699	2363	2616	2898
$F^2(4f^{N-1})$			76598	83474	89303	83509	93734	101777	104773	106963
$F^4(4f^{N-1})$			55728	60768	64165	74770	66918	71190	72351	73841
$F^6(4f^{N-1})$			38709	43210	44330	46575	48169	50316	50954	51997
$\zeta(4f^{N-1})$		827	974	1270	1434	1621	1823	2506	2768	3058
α		22	21	22	17	37	18	18	19	
β		−544	−641	−717	−640	−1905	−514	−655	−730	
γ		1520	1654	1564	1750	1679	1738	2500	2716	
M^0		1.8	2.0	2.1	2.4	1.6	4.4	4.1	3.8	
P^2		275	158	260	245	0	1003	510	43	
T^2			375	256	370		132	120	120	
T^3			42	26	40		25	50	50	
T^4			66	22	40		22	56	56	
T^6			−279	−141	−330		−317	−286	−286	
T^7			373	246	380		347	191	191	
T^8			285	382	370		162	176	176	
B_4	2208	2290	1987	1855	1928	1776	1671	1555	1787	1454
B_6	250	236	257	260	247	139	207	154	170	79
E_{exc}	34326	41210	47700	59900	64300	67440	73580	82650	84700	89200
$B_4(d)$	38709	38392	38076	37442	37126	36809	36500	35543	35200	34900
η_{fd}		0.53	0.53	0.53	0.53	0.53	0.53	0.53	0.53	0.53
ζ_{5d}	792.7	874	925	1028	1080	1132	1185	1346	1400	1453

Note. Refer to the text for explanation.

was the fitted value for Tb^{3+}. The parameter ζ_{5d} for Tb^{3+} is fitted to be 1185 cm^{-1}[28] which is 0.761 times the *ab initio* value 1557 cm^{-1}.[23] Hence this ratio was employed for all other ions. The parameter $B_4(d)$ was chosen to be linearly decreasing for $4f^N$ ions using $B_4(d, Ce) \times [1 - c \times (N-1)]$, where $c = 8.18 \times 10^{-3}$ was calculated from the crystal-field parameter values for Ce^{3+} and Tm^{3+} in CaF_2.[24,25]

We observed in the excitation spectra additional features that correspond to band-to-band and charge-transfer (CT) transitions. The experimental data are summarized in Table 2, together with some previous measurements.[26–28] In this table, the onset energy of each 4f–5d transition has been predicted using Dorenbos' phenomenological methods:[29,30]

$$E_{4f-5d}(Ln2, host) = E_{4f-5d}(Ln1, host) + \Delta E_{4f-5d}(Ln2, Ln1), \quad (3)$$

with the CT energy predicted using

$$E_{CT}(Ln2, host) = E_{CT}(Ln1, host) + \Delta E_{CT}(Ln2, Ln1). \quad (4)$$

The values in parentheses in Table 2 for the onset energies of 4f–5d are those corresponding to spin-forbidden (SF) absorption. The values of ΔE_{4f-5d}[29] and ΔE_{CT}[30] are given relative to Ce^{3+} and Eu^{3+}, respectively, which have the lowest 4f–5d and CT energy, respectively. The measured $E_{CT} = 37453\ cm^{-1}$ for Eu^{3+} was used then to predict E_{CT} for other ions.

Since the 4f – 5d absorption spectra comprise electric-dipole–allowed transitions, Franck-Condon replicas are observed to high energy of the zero-phonon lines. The detailed vibronic structures are not well-resolved at the spectral resolution employed, so that we adopted the crude simulation proposed by Reid et al.,[2] i.e., by using Gaussian curves displaced towards higher energy from the zero-phonon lines by $E_{shift} = 600\ cm^{-1}$ and

TABLE 2. Data for Zero-Phonon Line Energies of the First 4f–5d Band, Charge Transfer Energies and Valence to Conduction Band Absorption Energies

Ln^{3+}	ΔE_{4f-5d}[a]	E_{4f-5d} (calc)[b]	E_{4f-5d} (exp)	ΔE_{CT}[c]	E_{CT} (calc)[d]	E_{CT} (exp)[e]	CB[f]
(Y^{3+})							57.2
Ce^{3+}	0	N.A.	28.2[g]				
Pr^{3+}	12.2	40.4	39.8[h]	21.9	59.4		64.6*
Nd^{3+}	22.7	50.9	49.6[i]	17.7	55.2		63.5
Pm^{3+}	25.7	53.9					
Sm^{3+}	26.5	54.7		9.1	46.5	43.7(?)	56.9
Eu^{3+}	35.9	64.1		0.0	37.4	37.4	56.6
Gd^{3+}	45.8	74.0					58.7*[j]
Tb^{3+}	13.2 (SF: 5.5)	41.4 (SF: 33.7)	41.4 (SF: 34.3)[k]				58.1 or 55.6
Dy^{3+}	25.1 (SF: 17.7)	53.3 (SF: 45.9)		16.6	54.0		
Ho^{3+}	31.8 (SF: 29.1)	60.0 (SF: 57.3)		19.5	56.9		
Er^{3+}	30.0 (SF: 27.0)	58.2 (SF: 55.2)		18.9	56.3	55.0	53.6
Tm^{3+}	29.0 (SF: 27.0)	57.2 (SF: 55.2)		14.3	51.7	48.1[j]	56.1*[j]
Yb^{3+}	38.0	66.2		3.8	41.2	39.6	58.9
Lu^{3+}	49.2	77.4					53.5[l]

Note. The units are $10^3\ cm^{-1}$. SF = spin-forbidden. The energies relate to SF transitions. Refer to the text for explanation.

[a]From Ref. [29], relative to Ce^{3+}

[b]From Eq. (3).

[c]From Ref. [30], relative to Eu^{3+}.

[d]From Eq. (4).

[e]This work.

[f]Following Ref. [32]: 0.5 eV (4033 cm^{-1}) has been added to the peak maximum in this region of the room-temperature excitation spectrum. This may be an under-estimation. Starred values are from 10 K spectra. The value for Pr^{3+} is from Ref. [26].

[g]Ref. [11] at 10 K.

[h]Ref. [26] at 10 K.

[i]Ref. [27] at 295 K and revised herein.

[j]Ref. [10].

[k]Ref. [28] at 10 K.

[l]Ref. [48].

$E_{width} = 1000\,cm^{-1}$, as estimated from the experimental spectra. These curves are displayed as full lines in the simulated spectra. For simplicity, the calculated absorption spectra refer to transitions from the lowest crystal field level of the electronic ground state in all cases. It is noted that transitions from excited crystal field levels may contribute intensity in the experimental spectra, which were recorded at temperatures between 10 K and 298 K. The package of fd programs written by Prof. M.F. Reid was used to perform all the calculations.

RESULTS AND DISCUSSION

Y^{3+}

It was useful to record and compare the excitation and emission spectra of Cs_2NaYCl_6 since this crystal host has been employed for several Ln^{3+}. Under high-energy excitation, core-valence transitions have been reported for $Cs_2LiLaCl_6$[31] and $Cs_2LiLuCl_6$.[32] Some other bands in Cs_2LiYCl_6 (at 278 nm;[33] 325 nm[34]) and Cs_2LiYBr_6 (at 278 nm[33]) have been attributed to emission from a self-trapped exciton. The first sharp onset in the slow time-resolved excitation spectra of self-trapped exciton luminescence of neat hexachloroelpasolites has been assigned to the "fundamental absorption."[35] The first maximum was attributed to the creation of bound electron–hole pairs, whereas the creation of free electrons in the conduction band (CB) and holes in the valence band (VB) (i.e., the location of the bottom of the conduction band) was estimated to be 8%[35] or 0.5 eV[32] higher. In the following, we generally refer to peak maxima instead, but we have employed this reasoning in Table 2 to estimate the relative locations of the CB of the series $Cs_2NaLnCl_6$. From electron paramagnetic resonance and electron nuclear double resonance studies, Pawlik and Spaeth[36] identified two types of center in X-irradiated Cs_2NaYCl_6: the Y^{2+} and V_k centers, which are stable up to 70 K and 150 K, respectively.

The spectrum of neat Cs_2NaYCl_6, recorded at Desy,[10] under 170-nm excitation at 11 K, comprised a broad band extending from 360 to 580 nm (FWHM 93 nm) with maximum intensity at 448 nm ($22285\,cm^{-1}$). The excitation spectrum, when monitoring at 435 nm, showed a weak band at 221 nm ($45152\,cm^{-1}$), with major peaks at, and to high energy of, 170 nm. In order to investigate further this unexpected spectrum, the experiments were repeated at Hsinchu, Taiwan. Since we anticipated that oxygen species contributed intensity to the spectrum, in the present case the powder directly from Morss Method E was employed, in addition to a polycrystalline sample that had been passed through the Bridgman furnace. The powder sample is more deliquescent due to its much greater surface-to-volume ratio. The room-temperature excitation and emission spectra of the two samples are shown under different experimental conditions in Figure 1a,b. The powder spectra were much noisier than the crystal spectra due to nonradiative losses. For the powder sample, the excitation spectra show additional bands between 240 and 260 nm, presumably due to Y-O species, and the features in the emission spectra shifted to higher energy, with maximum at 340 nm, which is similar to the emission of neat Y_2O_3. The room-temperature emission spectrum of the crystal sample shows at least three broad bands with maxima at 382, 426 and 472 nm. Due to the overlap of these broad bands, it is not possible to monitor each one exclusively. A shorter wavelength overlapping band is partially resolved in the 25-K excitation spectrum of the crystal, in Fig. 1d. At least for the two longer wavelength (>420 nm) and two shorter wavelength (<400 nm) emission bands, the excitation and emission spectra appear to indicate a different origin for each set of these bands. In particular, the 382-nm band monitored in Fig. 1a for the crystal shows a greater contribution from the (lower energy) defect site excitation band at 198 nm. The major peaks in the 25-K crystal excitation spectra are between 176 and 178 nm, in Fig. 1c, which indicates a substantial shift of ~10 nm to shorter wavelength from the room-temperature spectra, in Fig. 1a.

Nd^{3+}

The synchrotron radiation excited emission and excitation spectra of $Cs_2NaNdCl_6$ further illustrate the problems in the interpretation of the hexachloroelpasolite spectra. For $Cs_2NaNdCl_6$ and Cs_2NaYCl_6: Nd^{3+}, $4f^3$–$4f^3$ emission has previously been reported from the multiplets $^4D_{3/2}$[16,27] at $27617\,cm^{-1}$, $^4G_{5/2}$ ($16690\,cm^{-1}$), and $^4F_{3/2}$ ($11336\,cm^{-1}$).[16] From the energy gaps between higher multiplet terms,[16] intraconfigurational emission could possibly be

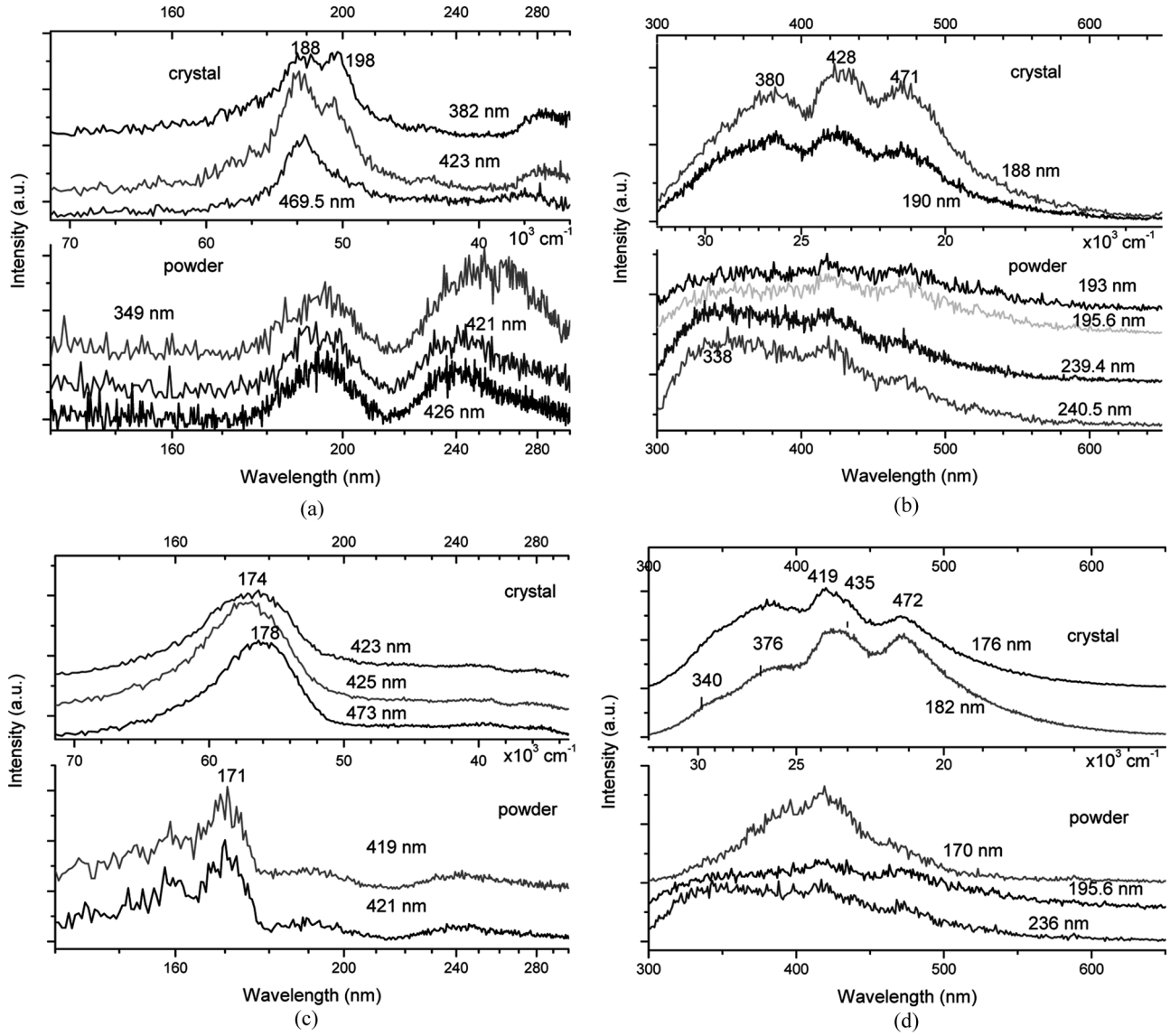

FIGURE 1 **Excitation (a), (c) and emission (b), (d) spectra of Cs_2NaYCl_6 powder and crystal samples at 298 K [(a), (b)], and 25 K [(c), (d)]. The excitation or monitored emission wavelengths are marked (nm), in addition to the locations of some peaks. The relative intensities are arbitrary.**

envisaged to occur from $^2F(2)_{5/2}$ at 37838 cm^{-1}. Interconfigurational emission was not previously detected at room temperature,[27] and this may be understood from the overlap of the ladder of $4f^3$ energy levels with $4f^2$5d states.

Figure 2a shows the emission spectra of $Cs_2NaNdCl_6$ using two different excitation wavelengths. Under 340-nm excitation, the emission bands at 369 nm and 395 nm could be assigned to $^4D_{3/2} \rightarrow {}^4I_{9/2}$, $^4I_{11/2}$ transitions, respectively, but the relative intensities are not as expected, and furthermore the transition $^4D_{3/2} \rightarrow {}^4I_{13/2}$ is not observed.[27] These emission bands are more likely assigned to trace Ce^{3+} impurity. Under 244.5-nm excitation, the emission bands at 312 nm and 344 nm may arise from a trace Gd^{3+} impurity, reflecting the zero-phonon line and OH_2 vibronic origin, respectively. Since the Ce^{3+} and Gd^{3+} impurities are trace, the respective absorption bands are expected to be too weak to be observed in the excitation spectra. The excitation spectra of these emission bands are given in Fig. 2b, together with calculated 4f–5d absorption. At present, we are unable to give assignments for these bands.

The previously measured ground ($^4I_{9/2}$) and excited ($^4F_{3/2}$) state absorption spectra[27] were interpreted to show that the lowest $4f^2$5d level is located around 47000–48000 cm^{-1}, which is lower than the

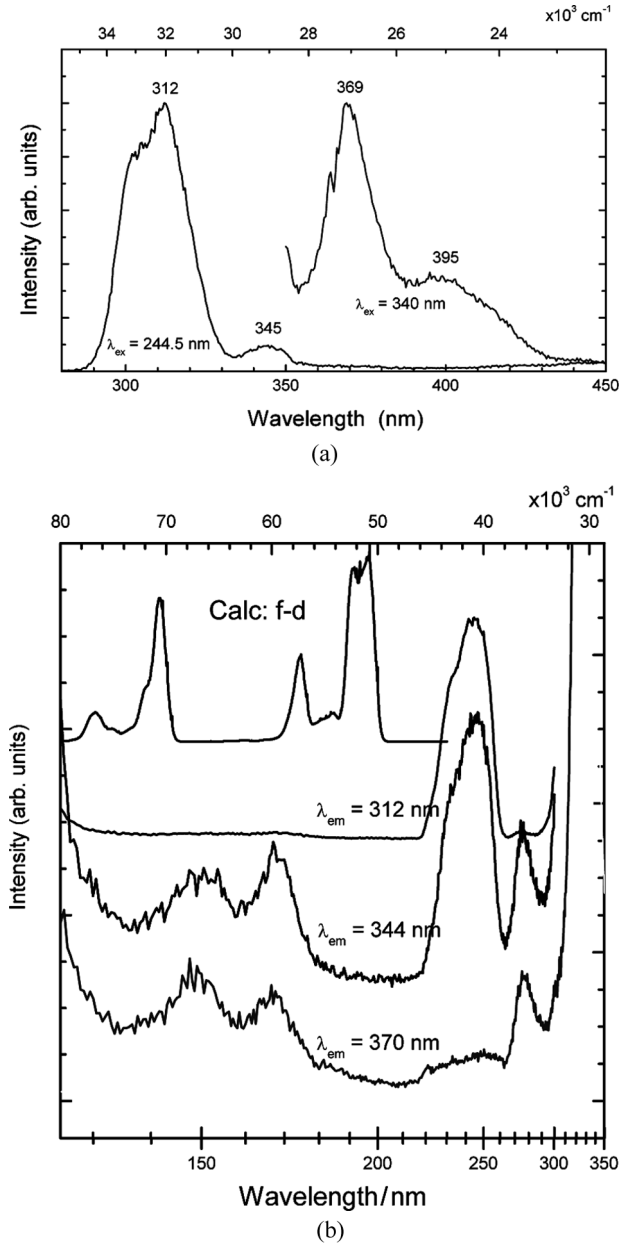

FIGURE 2 **Emission (a) and excitation (b) spectra of $Cs_2NaNdCl_6$ measured at room temperature, with the calculated f–d absorption spectrum in (b).**

predicted value 50000–50900 cm^{-1} by approximately 2000–4000 cm^{-1}. This discrepancy is larger than the estimated deviation of no more than 600 cm^{-1} given by Dorenbos, which was obtained from a systematic analysis of $4f^{N-1}5d$ levels in various hosts. A possible reinterpretation of the room-temperature spectra is that the maximum of the lowest energy band (207.3 nm) in the excited-state absorption spectrum corresponds to absorption from $^4H(2)_{9/2}$ (and not $^4F_{3/2}$), so that similarly, the 209.5-nm band in the ground state absorption spectrum corresponds to that from $^4I_{11/2}$ states. This would put the onset of $4f^25d$ states at 49600 ± 170 cm^{-1}. The Cl^- – Nd^{3+} CT band is predicted to be at approximately 55800 cm^{-1}.

Sm^{3+}

The spectra of neat $Cs_2NaSmCl_6$ and $Cs_2NaY_{1-x}Sm_xCl_6$ ($x = 0.1$ and 0.01) were investigated in this study. A comparison of the spectra of the neat and diluted ($x = 0.01$) elpasolites is given in Fig. 3. At room temperature, under excitation at 220–230 nm, weak emission is observed from $^4G_{5/2}$ located at 17742 cm^{-1} [37] to terminal states ^6H_J ($J = 5/2$, 7/2, and 9/2) as shown in Fig. 3a,b. A weak, broad band is observed at 333 nm for $Cs_2NaSmCl_6$ (Fig. 3a), and it is absent from the spectra of the $x = 0.01$ crystal (Fig. 3b). This feature could correspond to CT emission. The band at 371 nm in Fig. 3a is absent from the spectra of another sample of $Cs_2NaSmCl_6$ and is not considered further. The remaining emission peaks in the emission spectrum of $Cs_2NaSmCl_6$, between 389–472 nm at low temperature, are not prominent at room temperature (Fig. 3a,b), but are also observed at similar wavelengths in the low-temperature emission spectra of the $x = 0.01$ crystal under 192.6-nm or 225.6-nm excitation at 10 K (not shown), or 228.2-nm excitation at 10 K (Fig. 3b). These bands are also similar to those observed in Figs. 1b,d for Cs_2NaYCl_6 so that they do not correspond to transitions of yttrium or samarium chloride species or their related oxide impurities. The emission intensity of Sm^{3+} is several orders of magnitude greater in the $x = 0.01$ crystal compared with the neat crystal.

The excitation spectra of the Sm^{3+} emission from $^4G_{5/2}$ show a prominent band at 220–230 nm, which is close to the wavelength predicted in Table 2 for CT absorption (215 nm). However, the excitation into this band, which is within the band gap, also gives the emission bands between 380–480 nm, and the excitation band is much weaker for $Cs_2NaSmCl_6$ (Fig. 3c) than for $Cs_2NaY_{0.99}Sm_{0.01}Cl_6$. Features to shorter wavelength of 200 nm are also observed in the excitation spectra (Fig. 3c,d), and the "dip" marked at 186 nm (Fig. 3d) is similarly observed when monitoring the emission at 568.5 nm at 10 K. The peak maximum in the region of the band-to-band transition is near 192 nm.

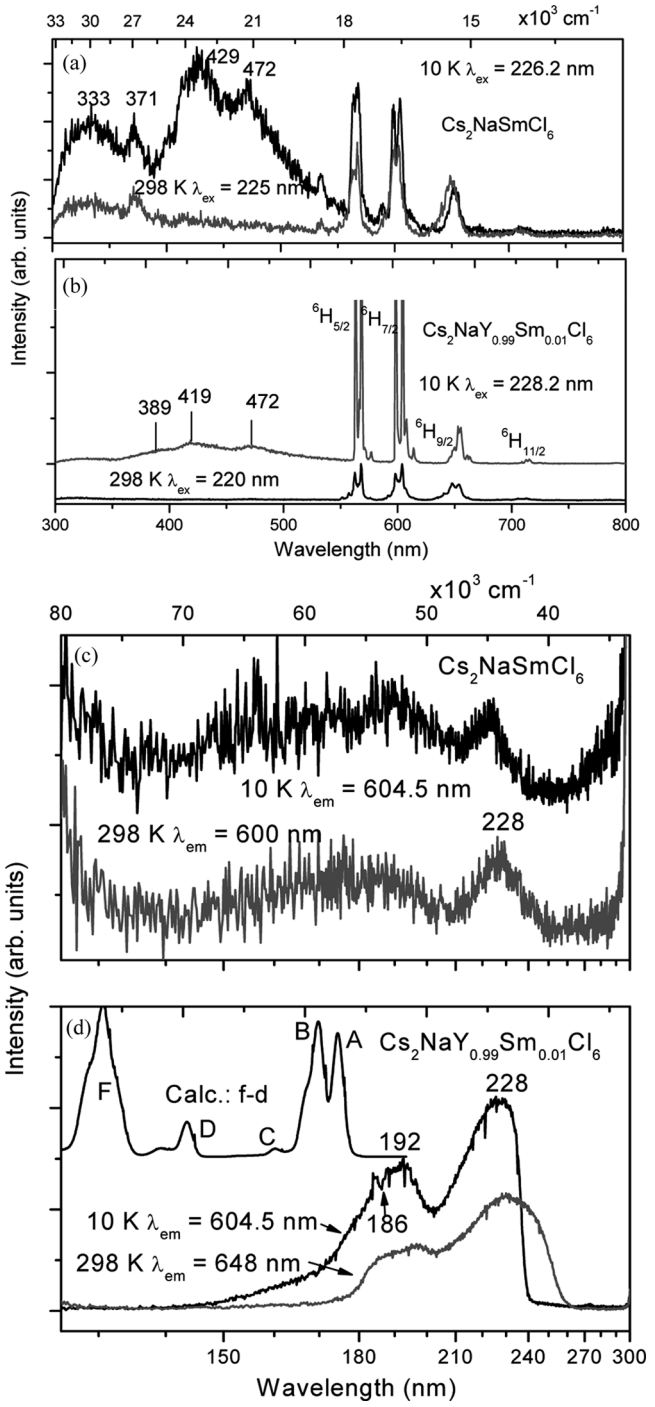

FIGURE 3 **Emission (a), (b) and excitation (c), (d) spectra of $Cs_2NaSmCl_6$ [(a), (c)] and $Cs_2NaY_{0.99}Sm_{0.01}Cl_6$ [(b), (d)]. The temperatures and excitation or emission wavelengths are marked. The calculated $4f^5 \rightarrow 4f^4 5d$ absorption spectrum is shown in (d), where A, B, C are absorptions to $^6(^5I,t_{2g})$; D to $^6(^5F,t_{2g})$; and F to $^6(^5I,e_{2g})$. The ordinate scale in the 10 K spectrum (b) is expanded to show the features between 389 and 472 nm.**

The calculated $4f^5$–$4f^4 5d^1$ absorption spectrum is also presented in Fig. 3d. The 4f–5d absorption is predicted to start at 54700 cm^{-1} (183 nm) and could account for the "dip" marked in this figure. The calculated f–d bands marked in Fig. 3d are due to absorption to $^6[(^5I)t_{2g}]$ $^6[(^5F)t_{2g}]$, and $^6[(^5I)e_{2g}]$ states for A-C, D, and F bands, respectively. Here, the strong valence-to-conduction-band absorption at energy above 190 nm does not permit the excitation of Sm^{3+} f–d absorption.

Eu^{3+}

The visible and ultraviolet emission spectra of Eu^{3+} in elpasolite hosts have been reported in several studies.[38–40] Under suitable excitation, emission occurs from ^5D_J ($J = 0$–3) to ^7F_J ($J = 0$–6) multiplets. Just as for the other systems studied herein, the vacuum ultraviolet excitation spectra of $Cs_2NaEuCl_6$ show considerable variation from sample to sample, although this is less so for the emission spectra. The excitation and emission spectra of $Cs_2NaEuCl_6$ recorded at Desy have previously been reported.[10]

The visible emission spectra of $Cs_2NaEuCl_6$ recorded for three different samples using various excitation lines are shown in Fig. 4a. For Sample i, emission is clearly observed from $^5D_0$ at room temperature and 10 K under excitation into the $Eu^{3+} - Cl^-$ charge transfer band. The $^5D_1$ emission increases markedly in intensity, relative to that from $^5D_0$, at the lower temperature. Emission from higher ^5D_J ($J = 2,3$) multiplets is quenched by ion–ion cross-relaxations in the neat crystals. Sample ii also shows a similar emission spectrum under 267.5-nm excitation, but impurity bands due to Tb^{3+} (at approximately 550 nm) are present under 170-nm excitation. This is shown by the excitation spectrum of 547.5-nm emission in Fig. 4b. The room-temperature spectrum of Crystal iii under 230-nm excitation shows additional bands at 312 nm (out of scale for this lowest spectrum in Fig. 4a) and a slightly stronger one at 366 nm with a shoulder at 412 nm. These bands are also present under 190.5-nm excitation, but are absent under 268-nm excitation. Although the latter two bands at 366 and 412 nm are essentially coincident with $CeCl_6^{3-}$ $5d \rightarrow 4f$ transitions, the excitation spectrum of the 366-nm band (Fig. 4b) shows a band at 248 nm that is not related to Ce^{3+} but more likely associated with $O^{2-} - Eu^{3+}$ CT.

Monitoring various Eu^{3+} emission bands from Samples i and ii at 298 K and 10 K (Fig. 4b) provides

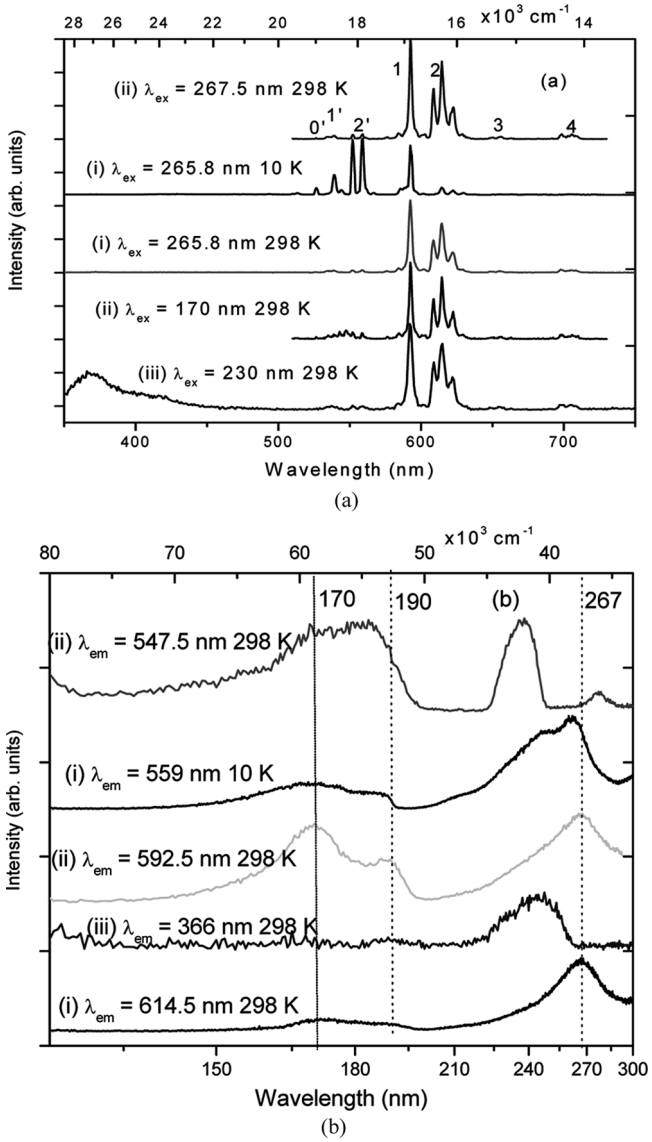

FIGURE 4 **Room-temperature and 10 K emission (a) and excitation (b) spectra of three samples [(i), (ii), (iii)] of $Cs_2NaEuCl_6$. In (a), the bands of transitions $^5D_1 \rightarrow {}^7F_J$, and $^5D_0 \rightarrow {}^7F_0$ are marked by J and J'.**

a more consistent picture. The $Cl^- - Eu^{3+}$ CT band is assigned at 267 nm. The final states of this transition involve a vibrationally excited $4f^7$ ground-state Eu^{2+} ion and a hole in the valence band. This band moves to higher energy in other spectra in Fig. 4b presumably due to substitution of the octahedral coordination of Eu^{3+} by varying amounts of oxide or hydroxide ion. The feature at 170 nm (i.e., at 21371 cm^{-1} higher in energy than the assigned $Cl^- - Eu^{3+}$ CT band) could be assigned the charge transfer to the $4f^65d$ excited state of Eu^{2+}. Finally, the maximum of the valence to conduction band transition is marked at 190 nm in Fig. 4b.

The simulated $4f^6 \rightarrow 4f^55d$ absorption spectrum of Eu^{3+} in $Cs_2NaEuCl_6$ has been displayed in Ref. [10]. The onset of f-d absorption is predicted to be at 64,100 cm^{-1} (156 nm), with strong features at 153, 147, 134, 119, and 109 nm, corresponding to transitions terminating at $^7(^6H, t_{2g})$, $^7(^6H, t_{2g})$, $^7(^6F, t_{2g}) + ^7(^6H, t_{2g})$, $^7(^6H, e_g)$, and $^7(^6F, e_g) + ^7(^6H, e_g)$, respectively.

Tb^{3+}

The low-energy electronic absorption spectra of $Cs_2NaTbCl_6$ and Cs_2NaYCl_6:Tb^{3+} have been previously reported and comprise spin-allowed (SA) and SF transitions.[28] Due to the extensive overlap of $4f^8$ levels with those of $4f^75d$, no d–f emission was anticipated or observed.

Figure 5a shows the room-temperature emission spectrum of $Cs_2NaTbCl_6$ under 186-nm excitation. The spectra using 240-nm and 280-nm excitations are the same and are also in agreement with the reported results of Faulkner and Richardson.[41] Emission from the $^5D_4$ multiplet of Tb^{3+}, with the lowest crystal field level Γ_1 located at 20468 cm^{-1}[42] to ^7F_J ($J = 6$–3) multiplets is observed between 480 and 640 nm, and the terminal states are marked in the figure.

The excitation spectra monitoring the strongest emission bands, at 547 nm and 543 nm, were measured and were indistinguishable. The former is presented in Fig. 5b, and the strong broad bands are saturated in intensity. Note that the "sticks" in Fig. 5b are calculated zero-phonon line positions and relative intensities, but refer to the absorption from the ground state $^7F_6\Gamma_1$, whereas the experimental excitation spectrum is at 298 K.

The zero-phonon lines of transitions to terminal states of Γ_{4u} irreducible representation were assigned from the previously reported absorption spectra of $TbCl_6^{3-}$[28] at (in cm^{-1}) 34332 (SF), 34982 (SF), 35590 (SF) and 41380 (SA). Hence, we assign the excitation bands in the ranges 265–295 nm and 230–250 nm to the SF and SA f–d absorptions, respectively. The first four lowest $4f^75d$ states are calculated to be within the energy range of 6 cm^{-1}[28] but transitions are only allowed to terminal states of Γ_{4u} representation. The weak bands at 320 nm and 305 nm can be assigned to absorption from thermally excited $^7F_4$ and $^7F_5$ multiplets, respectively.

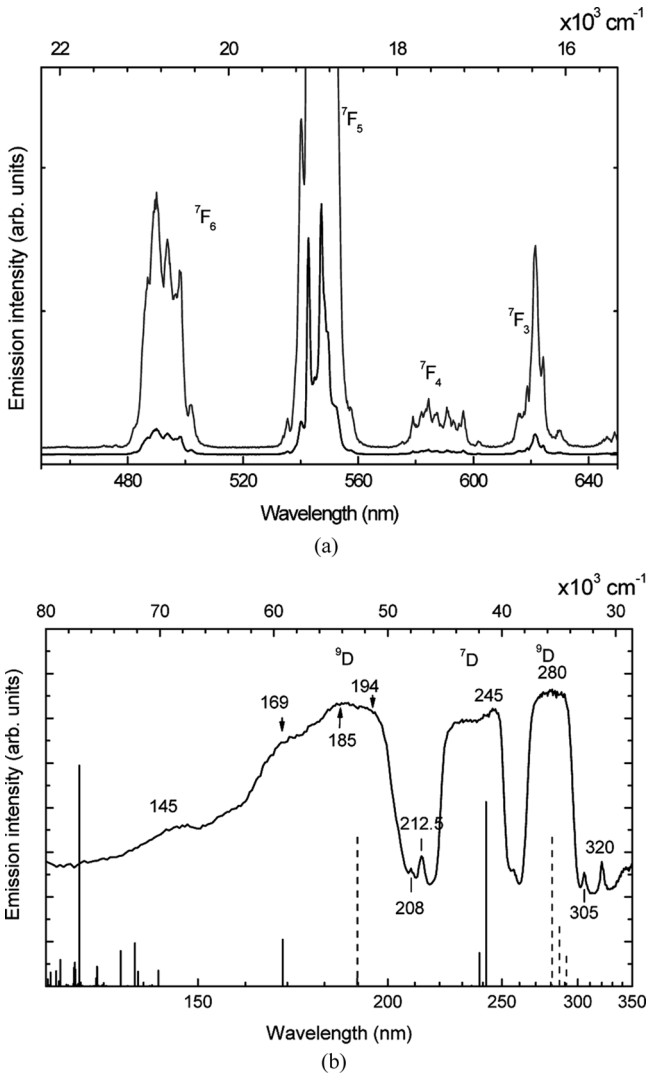

FIGURE 5 **Emission spectrum of $Cs_2NaTbCl_6$ excited at 186 nm (a) and excitation spectrum monitored at 547.25 nm (b). The initial luminescent state in (a) is $^5D_4$, and the ground state in (b) is $^7F_6$. Some terminal states are marked in both spectra. Some peak maxima are given in nm in (b), and the solid lines represent calculated spin-allowed absorption zero-phonon lines, whereas dashed lines are the positions of calculated spin-forbidden (SF) absorptions.**

Using the onset energies of these transitions (approximately 30800 cm^{-1} and 34650 cm^{-1}, respectively) and associating these energies with zero-phonon line transitions from the highest $^7F_4$ and $^7F_5$ crystal field levels (i.e., Γ_5 at 3673 cm^{-1} and $b\Gamma_4$ at 2349 cm^{-1}[18]) to the lowest $4f^7$5d state, the latter is estimated to be at 34560 ± 100 cm^{-1}, which is only approximately 130 cm^{-1} outside the measured[28] value of 34332 cm^{-1}. This error arises from the estimation of the onset using the experimental spectral bandpass of 130 cm^{-1}. It is interesting that the SA bands between 230 and 250 nm are followed at higher energy by a SF transition to a ^9D $4f^7$5d state. In fact, eight ^9D states are calculated to be within a range of ~100 cm^{-1},[28] but transitions from the electronic ground state are only allowed to two terminal Γ_{4u} states, separated by ~40 cm^{-1}. We can estimate the lowest energy ^9D state in this region by using an assignment, analogous to that above, of the weak bands at 212.5 nm and 208 nm to hot transitions from thermally excited $^7F_4$ and $^7F_5$ multiplets, respectively. Using the onset energies, as above, the lowest ^9D state, $^9[^8S,^2e_g]$, is then estimated to be at 50090 ± 100 cm^{-1}. For comparison, using the parameters given in Table 1, the next $4f^7$5d states are calculated to be $^9[^8S,^2e_g]$ in the range 52,566–52,691 cm^{-1} (~190 nm). The estimated value of 50,090 cm^{-1} is therefore ~2500 cm^{-1} lower than the calculated value.

The consequence of this re-assignment of the lowest energy level $^9[^8S,^2e_g]$ has not been incorporated into our parameter values in Table 1. However, it would result in the reduction of $B_4(d)$ by 11% from the value in Table 1 and an energy of $^7[^8S,^2e_g]$ that is lower by 2500 cm^{-1}, but no apparent changes for the other calculated $4f^7$5d levels mentioned above.

The SF transitions at ~190 nm are followed at higher energies by SA transitions to $^7[^8S,^2e_g]$ in the range 59217–59265 cm^{-1} (~169 nm), then by transitions to $^7[^6P,t_{2g}]$ in the range 69785–73760 cm^{-1} (143–136 nm), and many other $4f^7$5d states where the $4f^7$ core is in excited multiplets. The shoulders at 169 nm and 146 nm could be due to ground state absorptions to $^7[^8S,e_g]$ and $^7[^6P,t_{2g}]$ states, but otherwise these bands reflect conduction band states. The band at approximately 190 nm is likely due to the valence to conduction band absorption as well as to the SF absorption to $^9[^8S,^2e_g]$. The strong valence to conduction band absorption greatly reduces the penetrating depth of higher energy photons and hence the efficiency of excitation. As a consequence, the f–d SA excitation bands at higher energy are much weaker than the lower energy f–d excitation bands.

Er^{3+}

The room-temperature emission, excitation, and cross-relaxation processes of $Cs_2NaErCl_6$ have been presented in detail.[43] The room-temperature excitation and 10-K emission spectra were also recorded at Desy.[10] The latter spectrum was dominated by

emission from $^4S_{3/2}$ and transitions were also evident from $^2G_{9/2}$[10] were transitions that were not present at room temperature.[43] Herein we show, for comparison, the room-temperature emission spectra of $Cs_2NaErCl_6$ recorded using 183-nm and 201.5-nm excitations (Fig. 6a), as well as various excitation spectra of the neat and diluted systems (Fig. 6b).

From Table 2, the $Cl^- - Er^{3+}$ CT band is predicted to be at 55500 cm^{-1} (180 nm). Therefore the broad shoulder near this wavelength in the excitation spectra of $Cs_2NaErCl_6$ emission (Fig. 6b) is assigned to this transition. This shoulder disappears in the excitation spectrum of $Cs_2NaYCl_6:Er^{3+}$ (0.1 at.%), indicating that it depends on the concentration of Er^{3+}. The broad, stronger band in Fig. 6b is attributed to band-to-band absorption, which shifts from 201 nm for $Cs_2NaErCl_6$ to 189.5 nm for $Cs_2NaYCl_6:Er^{3+}$. The structure to low energy of this band in Fig. 6b corresponds to $4f^{11}$–$4f^{11}$ intraconfigurational transitions of Er^{3+}, and some of the terminal multiplet terms are marked in the figure. The "dip" marked by an arrow in the excitation spectra of $Cs_2NaErCl_6$ in Fig. 6b appears to be a Fano antiresonance. There is a broad host absorption band overlapped by a sharp f–f transition that does not populate the luminescent states.

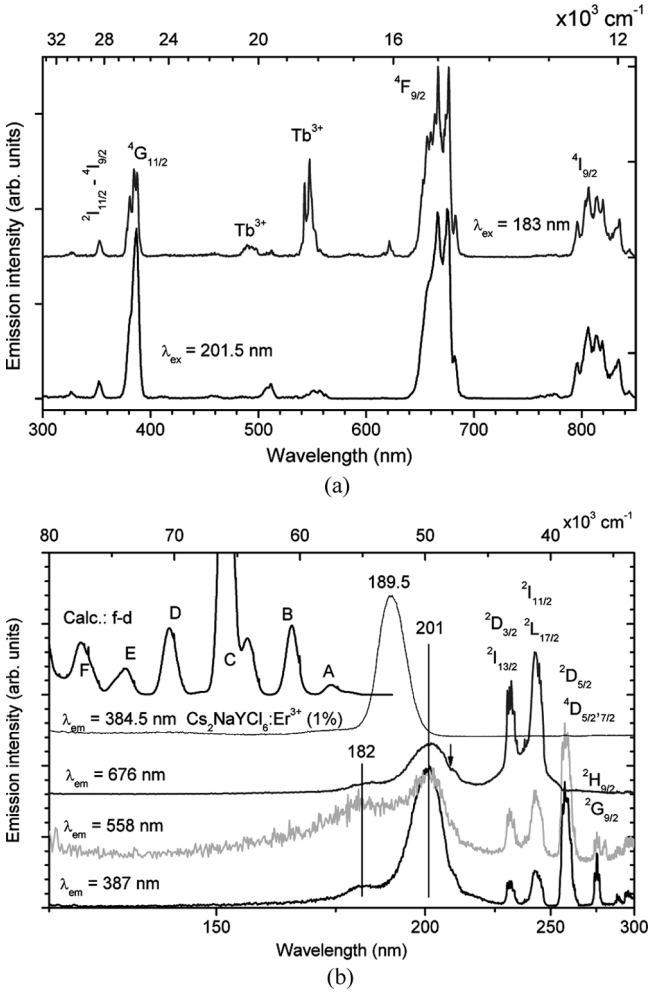

FIGURE 6 **Emission (a) and excitation (b) spectra of $Cs_2NaErCl_6$ measured at room temperature. The terminal multiplet terms are marked for some peaks: for these in (a), the terminal multiplet term is the ground term, $^4I_{15/2}$, except for $^2I_{11/2}$, where indicated. Some Tb^{3+} impurity emission bands are marked; for (b), the initial multiplet is $^4I_{15/2}$. The calculated f–d absorption spectrum is shown in (b) for comparison.**

The $4f^{11} \rightarrow 4f^{10}5d$ absorption transitions are predicted, using Dorenbos method, to start at 55150 cm^{-1} (181 nm: SF transition) and 58200 cm^{-1} (172 nm: SA transition). Detailed calculation shows that most of the states have considerable spin admixture. The first few peaks in Fig. 6b are A, dominated by $^6[(^5I)t_{2g}]$; B, $^6[(^5I)t_{2g}]$ with a considerable mixture of $^4[(^5I)t_{2g}]$; C and D, $^4[(^5I)t_{2g}]$; E and F, $^6[(^5F)t_{2g}]$. Since the $4f^{10}5d$ energies lie above the band gap, the interconfigurational transitions are not observed.

The room-temperature emission spectra of $Cs_2NaErCl_6$ were recorded using excitation into the charge transfer band (top spectrum, Fig. 6a) and using band-to-band excitation (bottom spectrum). There are significant differences in the relative intensities of spectral features in these emission spectra. For example, transitions from $^4G_{11/2}$ are enhanced under 201.5-nm excitation, relative to those from $^4F_{9/2}$ under 183-nm excitation. The Tb^{3+} impurity emissions in Fig. 6a are not related to the $Cs_2NaErCl_6$ sample, but to stray emission from an adjacently mounted $Cs_2NaTbCl_6$ sample.

Yb^{3+}

The excitation and emission spectra of $Cs_2NaYbCl_6$ were recorded at Desy,[10] but the spectral features mainly originated from trace Tm^{3+} impurity. Other species or trace impurities are still observed in the present emission spectra.

The zero-phonon line of the first 4f–5d absorption band is predicted to be at 66200 cm^{-1} using the method given by Dorenbos.[29] Calculations using the parameters given in Table 2 show that most $4f^{12}5d$ states are of mixed-spin nature, except the lowest few levels, which are of high-spin ($S = 3/2$) parentage and appear as a tail ranging from 63500 cm^{-1} (157 nm) to the first absorption peak in

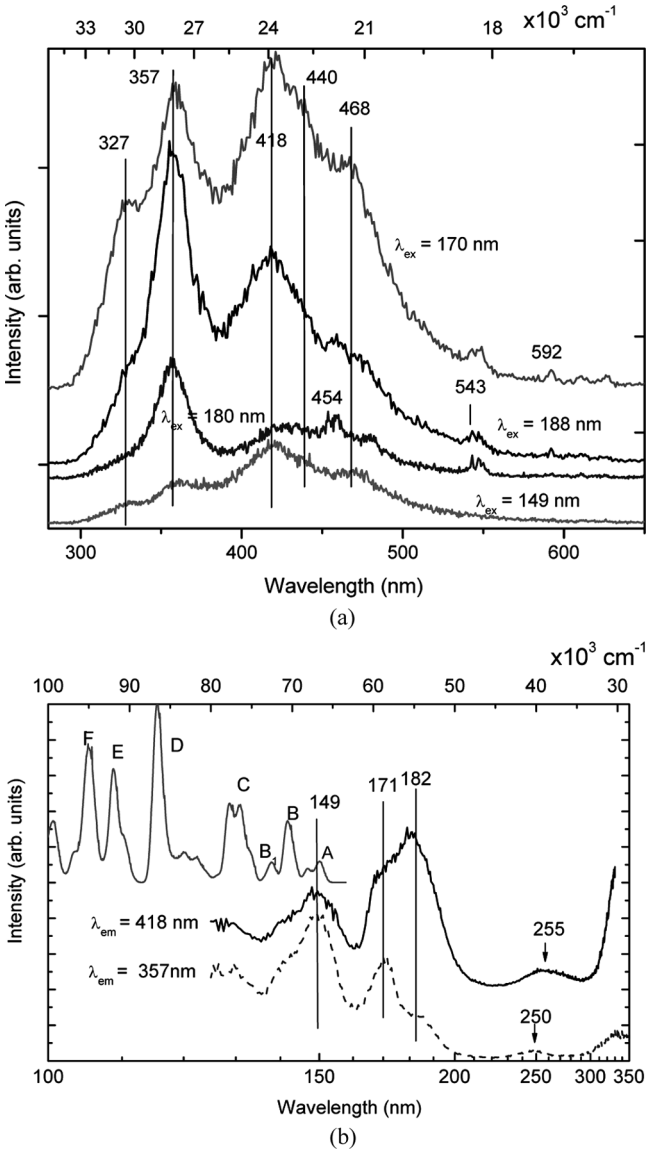

FIGURE 7 **Emission (a) and excitation (b) spectra of $Cs_2NaYbCl_6$ at room temperature.**

the calculated absorption spectrum. In the calculated absorption spectrum (Fig. 7b), peaks A, B, B_1, and C are dominated by transitions to terminal states of $^2(^3H_6, t_{2g})$, $^2(^3H_5, t_{2g})$, $^2(^3F_4, t_{2g})$, and $^2(^3H_4, t_{2g})$ characteristics, respectively; D and F are of $^2(^3H_6, e_g)$ and $^2(^3H_5, e_g)$ parentage, and E comprises $^2(^1G_4, t_{2g})$.

From Table 2, the CT band is predicted to be at low energy, at 41,200 cm^{-1}. The excitation spectra monitoring 357-nm and 418-nm emissions are shown in Fig. 7b. The weak band centered at 250–255 nm (40000–39220 cm^{-1}) is therefore assigned to Cl^- – Yb^{3+} CT absorption. The 182-nm feature is associated with the band-to-band transition. A further feature at 149 nm is at ~28,000-cm^{-1} higher energy than the CT band, and could be assigned to the CT transition to the $4f^{13}5d$ state of Yb^{2+} since the lowest energy bands in the $4f^{14} \rightarrow 4f^{13}5d$ absorption transition of Yb^{2+} in $SrCl_2$ have been located at ~27,000 cm^{-1}.[44] If this assignment is correct, it is interesting that this transition is observed although it has energy much higher than that of the band gap, whereas the $4f^{13} \rightarrow 4f^{12}5d$ transitions of Yb^{2+} are not present.

The emission spectra under several different excitation wavelengths are displayed in Fig. 7a. The spectra contain structured broad bands with two major peaks at 357 nm and 418 nm. These bands are not related to the f–f emission of Yb^{3+} single ions or dimers and are further discussed in the conclusions section.

Certainly, some other impurity bands are present in Fig. 7a, indicating traces of Er^{3+} (marked at 543 nm) and Eu^{3+} (marked at 592 nm), but the intensities are very weak, especially in comparison with the Desy spectrum.[10]

CONCLUSIONS

With the exceptions of Ce^{3+} and Pr^{3+}, no d–f emissions are observed for the series $Cs_2NaLnCl_6$. This is either due to the position of the d-electron levels above the host band gap, or to fast nonradiative decay to the overlapping ladder of f-electron energy levels. As in the preliminary study at Desy,[10] the excitation spectra presented herein highlight the occurrence of impurity bands and other features that are apparently unrelated to the Ln^{3+} ion in $Cs_2NaLnCl_6$. Some of the impurity bands have been assigned to various oxygen-coordinated species in these deliquescent materials, as in the cases of Eu^{3+} herein and Ce^{3+} in Ref. [10], whereas other bands in the excitation or emission spectra are due to inadvertent traces of other lanthanide ions, as for Nd^{3+}, Eu^{3+}, Yb^{3+} herein, and Gd^{3+} and Yb^{3+} in Ref. [10].

Besides the presence of other lanthanide ions, for some other bands it is necessary to distinguish whether they are due to an intrinsic center or to a defect. The difference between these two choices is that the electronic ground state is that of the pure crystal for the former, but of a defect for the latter. The first choice appears to be excluded for the emission bands at ~380, 420, 440, and 470 nm because

they are at very similar locations in $Cs_2NaLnCl_6$ (Ln = Y, Sm, Yb) and most likely correspond to the same emitting species. The excitation spectra of the 420-nm emission band for Ln = Y and Yb (Fig. 1, Fig. 7) exhibit a prominent feature near the band gap in each case. The assignment of the emission bands to a self-trapped exciton is also excluded since it is then difficult to explain the multiplicity of emission bands. A second possibility is the assignment of these bands to emission from the $^5D_3$ state of trace Tb^{3+} impurity ($^5D_3$ Γ_5 is at 26261 cm^{-1}[19]) to ^7F_J levels. The emission from $^5D_3$ is not apparent in *neat* $Cs_2NaTbCl_6$ at room temperature[45] (compare with Fig. 5a) and is probably quenched by a temperature-dependent cross-relaxation process. However, the reported 355-nm excited 10-K emission spectrum of $Cs_2NaTbCl_6$ in the region 370–480 nm [46] shows, in addition to the fine structure of the emission from $^5D_3$, some underlying broad bands with maxima at ~429 nm and 405 nm that could correspond to the broad features observed herein at room temperature. The nature of the emission bands therefore remains unsolved.

Charge transfer absorption bands have been assigned from experimental data in Table 2 at the wavelengths of 267 nm for Eu^{3+}, 228 nm for Sm^{3+}, 182 nm for Er^{3+}, 253 nm for Yb^{3+}, and—in Ref. [10]—177 nm for Er^{3+} and 208 nm for Tm^{3+}. The assignments were purely made on the basis of reasonable agreement of observed features with calculated locations of CT bands, and only the assignment for Eu^{3+} is considered secure. For comparison, Ryan and Jørgensen[47] gave the following wavelengths for CT absorption bands for "hexahalides" in nitrile solution: 301 nm for Eu^{3+}, 232 nm for Sm^{3+}, and 273 nm for Yb^{3+}. Although the assignment of the π – d CT bands for Eu^{3+} and Yb^{3+} appears to be reasonable on energy arguments, the apparent absence of this transition for Sm^{3+} (Fig. 3d) cannot be readily explained. It is clear from the present study that the structure to wavelengths that are shorter than ~180 nm in the previously reported synchrotron excitation spectra of $Cs_2NaPrCl_6$ and Cs_2NaYCl_6:Pr^{3+}[26] is more likely associated with the host lattice transitions than CT or with $4f^2 \rightarrow 4f^15d^1$ transitions.

Figure 8 shows the relative locations of the ground (or vibrationally excited ground for Ln^{2+} since it is based on the CT for Eu^{3+}) state levels of the

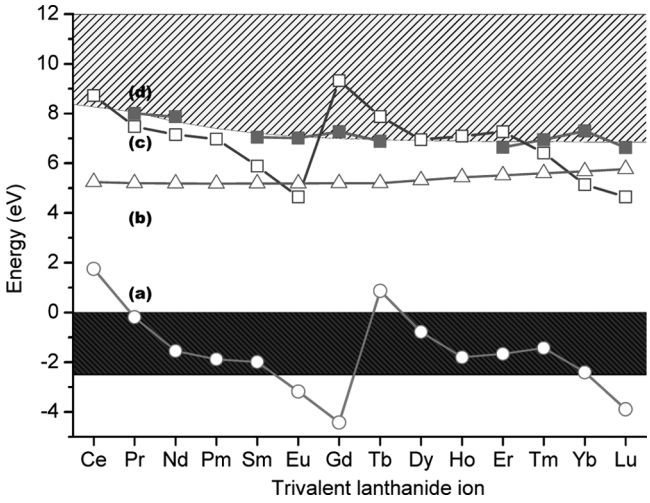

FIGURE 8 **Energy diagram for $Cs_2NaLnCl_6$ relative to the top of the valence band. The band gaps in curve (d) were taken from Table 2 and are then smoothed and interpolated for all Ln^{3+}. Curve (a) represents the absolute position of the Ln^{3+} $4f^N$ ground state; (b) the absolute position of the lowest Ln^{3+} $4f^{N-1}5d$ state; and (c) the absolute position of the Ln^{2+} $4f^N$ vibrationally excited ground state. The energies in curves (a) to (c) are defined as the difference of the binding energy of the electron in the valence band from the last-filled electron in the lanthanide ion. For example, the $4f^8$ configuration of Gd^{2+} is at ~9.3 eV, which means that it needs 9.3 eV less energy to ionize a 4f electron of Gd^{2+} ($4f^8$) then it does for a valence band electron.**

configurations Ln^{3+} $4f^N$, Ln^{2+} $4f^{N+1}$, and Ln^{3+} $4f^{N-1}5d$, relative to the VB. The CT energies in Table 2 and in Fig. 8 are calculated from the value for the CT wavelength of Eu^{3+} (267 nm) and represent the transitions:

$$Ln^{3+}\ (\text{ground state}) + \text{VB (top)} \rightarrow Ln^{2+} \\ (\text{excited vibrational state}) + \text{VB (hole)}. \quad (5)$$

The location of the $4f^N$ ground state of Ln^{3+} relative to the top of the VB is estimated from that of Lu^{3+} in $Cs_2LiLuCl_6$ (−3.9 eV) [32,48] with the widths of the VB and CB being about 3 eV and 8 eV, respectively,[31] from $Cs_2LiLaCl_6$. The energies of the $4f^{N-1}5d$ ground states of Ln^{3+} are deduced from the $5d^1$ energy level of Ce^{3+}. The estimated locations of the CB for the series $Cs_2NaLnCl_6$, including Ln = Y and Lu are also included in the figure. The CB energies follow the reasoning of Bessière et al.,[32] where 0.5 eV has been added to the energy of the strong band in the excitation spectrum in this region at room temperature. Rodnyi et al.[31] noted that the band gap should decrease with increasing temperature for $Cs_2LiLaCl_6$:Ce^{3+} since it is inversely proportional to the square of the anion–cation

separation. There is not a systematic increasing trend of band gap energy in Table 2 throughout the $Cs_2NaLnCl_6$ series with decreasing lattice parameter, just as for Ln_2O_3,[49] so that other factors also play a role.

ACKNOWLEDGMENTS

Financial support for this work from the Hong Kong Research grants Council General Research Fund Grant City U. 102308 is gratefully acknowledged. This work was also supported by the National Science Foundation of China, under Grant 10874253.

REFERENCES

1. Peijzel, P. S.; Meijerink, A.; Wegh, R. T.; Reid, M. F.; Burdick, G. W. A complete $4f^n$ energy level diagram for all trivalent lanthanide ions. *J. Solid State Chem.* **2005**, *178*, 448–453.
2. Reid, M. F.; van Pieterson, L.; Wegh, R. T.; Meijerink, A. Crystal field parameters from ab initio calculations. *Phys. Rev. B.* **2000**, *62*, 14744–14749.
3. Kirm, M.; Stryganyuk, G.; Vielhauer, S.; Zimmerer, G.; Makhov, V. N.; Malkin, B. Z.; Solovyev, O. V.; Abdulsabirov, R. Yu.; Korableva, S. L. Vacuum ultraviolet 5d–4f luminescence of Gd^{3+} and Lu^{3+} ions in fluoride matrices. *Phys. Rev. B.* **2007**, *75*, art. no. 075111.
4. Malkin, B. Z.; Solovyev, O. V.; Malishev, A. Y.; Saikin, S. K. Theoretical studies of electron-vibrational $4f^N$–$4f^{N-1}5d$ spectra in $LiYF_4:RE^{3+}$ crystals. *J. Lumin.* **2007**, *125*, 175–183.
5. Collombet, A.; Guyot, Y.; Joubert, M. F.; Laroche, M.; Margerie, J.; Moncorgé, R.; Descroix, E. Experimental and theoretical investigation of $4f^3$–$4f^25d$ interconfigurational transitions in $Nd^{3+}:LiYF_4$ crystals. *Phys. Rev. B.* **2003**, *68*, art. no. 035115.
6. Belsky, A. N.; Krupa, J. C. Luminescence excitation mechanisms of rare earth doped phosphors in the VUV range. *Displays.* **1999**, *19*, 185–196.
7. Lushchik, A.; Lushchik, C.; Kotlov, A.; Kudryavtseva, I.; Maaroos, A.; Nagirnyi, V.; Vasil'chenko, E. Spectral transformers of VUV radiation on the basis of wide-gap oxides. *Rad. Meas.* **2004**, *38*, 747–752.
8. van der Kolk, E.; Dorenbos, P.; van Eijk, C. W. E. Vacuum ultraviolet excitation of $^3P_0$ and $^1S_0$ emission of Pr^{3+} in $Sr_{0.7}La_{0.3}Al_{11.7}Mg_{0.3}O_{19}$ and SrB_4O_7. *J. Phys.: Condens. Matt.* **2001**, *13*, 5471–5486.
9. Yen, W. M.; Raukas, M.; Basun, S. A.; van Schaik, W.; Happek, U. Optical and photoconductive properties of cerium-doped crystalline solids. *J. Lumin.* **1996**, *69*, 287–294.
10. Duan, C.-K.; Tanner, P. A.; Meijerink, A.; Babin, V. Synchrotron excitation, emission and theoretical simulation of lanthanide ions in hexachloroelpasolite crystals. *J. Phys.: Condens. Matter.* **2009**, *21*, art. no. 395501.
11. Tanner, P. A.; Mak, C. S. K.; Edelstein, N. M.; Liu, G.; Huang, J.; Seijo, L.; Barandiarán, Z. Absorption and emission of Ce^{3+} in elpasolite lattices. *J. Am. Chem. Soc.* **2003**, *125*, 13225–13233.
12. Lu, H.-C.; Chen, H.-K.; Tseng, T.-Y.; Kuo, W.-L., Alam, M. S.; Cheng, B.-M. Photoluminescence of phosphors for PDP with VUV excitation. *J. Electron Spectrosc. Relat. Phenom.* **2005**, *144–147*, 983–985.
13. Song, Y. F.; Ma, C.-I.; Hsieh, T.-F.; Huang, L.-R.; Chung, S.-C.; Cheng, G. Y. Hsiung, N.-F.; Wang, D.-J.; Chen, C. T.; Tsang, K.-L. Performance of a novel VUV bending magnet beamline. *Nucl. Instr. Method Phys. Res. A.* **2001**, *467–468*, 569–572.
14. Duan, C.-K.; Tanner, P. A.; Babin, V.; Meijerink, A. Theoretical simulation and synchrotron excitation spectra of lanthanide ions in hexafluoroelpasolite lattices. *J. Phys. Chem. C.* **2009**, *113*, 12580–12585.
15. Reid, M. F.; Richardson, F. S. Free ion, crystal-field, and spin-correlated crystal-field parameters for lanthanide ions in $Cs_2NaLnCl_6$ and $Cs_2NaYCl_6:Ln^{3+}$ systems. *J. Chem. Phys.* **1985**, *83*, 3831–3836.
16. Zhou, X. J.; Mak, C. S. K.; Tanner, P. A.; Faucher, M. D. Spectroscopic properties and configuration interaction assisted crystal field analysis of Nd^{3+} in neat $Cs_2NaNdCl_6$. *Phys. Rev. B.* **2006**, *73*, art. no. 075113.
17. Faucher, M. D.; Tanner, P. A. Energy levels and hypersensitivity of samarium(III) in the elpasolite $Cs_2NaSmCl_6$. *J. Phys.: Condens. Matter.* **2006**, *18*, 8503–8522.
18. Tanner, P. A.; Ravi Kanth Kumar, V. V.; Jayasankar, C. K.; Reid, M. F. Analysis of spectral data and comparative energy level parametrizations for Ln^{3+} in cubic elpasolite crystals. *J. Alloys Compds.* **1994**, *215*, 349–370.
19. Morrison, I. D.; Berry, A. J.; Denning, R. G. Energy levels of terbium(III) in the elpasolite $Cs_2NaTbCl_6$. *Mol. Phys.* **1999**, *96*, 43–51.
20. Tanner, P. A.; Mak, C. S. K.; Kwok, W.-M.; Phillips, D. L.; Faucher, M. D. Ultraviolet f–f emission and crystal field analysis for Er^{3+} in $Cs_2NaErCl_6$. *Phys. Rev B.* **2002**, *66*, art. no. 165203.
21. Faucher, M. D.; Tanner, P. A.; Mak, C. S. K. Electronic spectra and configuration interaction of Tm^{3+} in $TmCl_6^{3-}$. *J. Phys. Chem. A.* **2004**, *108*, 5278–5287.
22. Zhou, X. J.; Reid, M. F.; Faucher, M. D.; Tanner, P. A. Electronic spectra of Cs_2NaYbF_6 and crystal field analyses of YbX_6^{3-} (X=F, Cl, Br). *J. Phys. Chem. B.* **2006**, *110*, 14939–14942.
23. Reid, M. F.; van Pieterson, L.; Meijerink, A. Trends in parameters of the $4f^N$–$4f^{N-1}5d$ spectra of lanthanide ions in crystals. *J. Alloys Compds.* **2002**, *344*, 240–245.
24. van Pieterson, L.; Reid, M. F.; Wegh, R. T.; Soverna, S.; Meijerink, A. $4f^n$–$4f^{n-1}5d$ transitions of the light lanthanides: Experiment and theory. *Phys. Rev. B.* **2002**, *65*, art. no. 045113.
25. van Pieterson, L.; Reid, M. F.; Burdick, G. W.; Meijerink, A. $4f^n$–$4f^{n-1}5d$ transitions of the heavy lanthanides: Experiment and theory. *Phys. Rev. B.* **2002**, *65*, art. no. 045114.
26. Tanner, P. A.; Mak, C. S. K.; Faucher, M. D.; Kwok, W.-M.; Phillips, D. L.; Mikhailik, V. 4f–5d transitions of Pr^{3+} in elpasolite lattices. *Phys. Rev. B.* **2003**, *67*, art. no. 115102.
27. Collombet, A.; Guyot, Y.; Mak, C. S. K.; Tanner, P. A.; Joubert, M.-F. Spectroscopic investigation of the Nd^{3+} $4f^25d$ states in chloroelpasolite crystals. *J. Lumin.* **2001**, *94–95*, 39–43.
28. Ning, L. X.; Mak, C. S. K.; Tanner, P. A. High spin and low spin f–d transitions of Tb^{3+} in elpasolite hosts. *Phys. Rev. B.* **2005**, *72*, art. no. 085127.
29. Dorenbos, P. 5d level positions of the trivalent lanthanides in inorganic compounds. *J. Lumin.* **2000**, *91*, 155–176.
30. Dorenbos, P. Lanthanide charge transfer energies and related luminescence, charge carrier trapping, and redox phenomena. *J. Alloys Compds.* **2009**, *488*, 568–573.
31. Rodnyi, P. A.; Mikhailik, V. B.; Stryganyuk, G. B.; Voloshinovskii, A. S.; van Eijk, C. W. E.; Zimmerer, G. F. Luminescence properties of Ce-doped $Cs_2LiLaCl_6$ crystals. *J. Lumin.* **2000**, *86*, 161–166.
32. Bessière, A.; Dorenbos, P.; van Eijk, C. W. E.; Krämer, K. W.; Güdel, H. U.; Galtayries, A. Scintillation and anomalous emission in elpasolite $Cs_2LiLuCl_6:Ce^{3+}$. *J. Lumin.* **2006**, *117*, 187–198.
33. van Loef, E. V. D.; Dorenbos, P.; van Eijk, C. W. E.; Krämer, K. W.; Güdel, H. U. Scintillation and spectroscopy of the pure and Ce^{3+}-doped elpasolites: Cs_2LiYX_6 (X=Cl, Br). *J. Phys.: Condens. Matter.* **2002**, *14*, 8481–8496.
34. Bessière, A.; Dorenbos, P.; van Eijk, C. W. E.; Pidol, L.; Krämer, K. W.; Güdel, H. U. Spectroscopy and anomalous emission of Ce-doped elpasolite Cs_2LiYCl_6. *J. Phys:. Condens. Matter.* **2004**, *16*, 1887–1897.
35. Birowosuto, M. D.; Dorenbos, P.; van Eijk, C. W. E.; Krämer, K. W.; Güdel, H. U. Scintillation properties and anomalous Ce^{3+} emission of $Cs_2NaREBr_6:Ce^{3+}$ (RE=La, Y, Lu). *J. Phys.: Condens. Matter.* **2006**, *18*, 6133–6148.
36. Pawlik, Th.; Spaeth, J.-M. Electron and hole centres in the X-irradiated Cs_2NaYCl_6 elpasolite crystal studied by means of electron

paramagnetic resonance and electron nuclear double resonance. *J. Phys.: Condens. Matter.* **1997**, *9*, 8737–8747.
37. Tanner, P. A. Vibronic analysis of the $(^4G_{5/2})$ Γ_8 – $^6H_{5/2}$,$^6H_{7/2}$, $^6H_{9/2}$ luminescence transitions of Cs_2NaYCl_6:$SmCl_6^{3-}$. *Chem. Phys. Lett.* **1989**, *155*, 59–62.
38. Serra, O. A.; Thompson, L. C. Emission spectra of $Cs_2NaEuCl_6$ and $Cs_2Na(Eu,Y)Cl_6$. *Inorg. Chem.* **1976**, *15*, 504–507.
39. Flint, C. D.; Stewart-Darling, F. L. Vibronic transitions in the luminescence spectrum of $Cs_2NaEuCl_6$. *Molec. Phys.* **1981**, *44*, 61–68.
40. Morley, J. P.; Faulkner, T. R.; Richardson, F. S. Optical emission spectra and crystal field analysis of Eu^{3+} in the cubic Cs_2NaYCl_6 host. *J. Chem. Phys.* **1982**, *77*, 1710–1733.
41. Faulkner, T. R.; Richardson, F. S. Magnetic dipole and vibronically-induced electric dipole transition intensities of the $^5D_4$–^7F_J transitions of Tb^{3+} in $Cs_2NaTbCl_6$. *Molec. Phys.* **1978**, *36*, 193–214.
42. Tanner, P. A.; Liu, Y. L.; Chua, M.; Reid, M. F. Nonresonant energy transfer from the $^5D_4$ level of Tb^{3+} to the $^5D_0$ level of Eu^{3+}. *J. Alloys Compds.* **1994**, *207/208*, 83–86.
43. Zhou, X.; Tanner, P. A.; Duan, C. K.; Cheng, B.-M. Downconversion in $Cs_2NaErCl_6$. *Chem. Phys. Lett.* **2007**, *442*, 302–306.
44. Pan, Z.; Duan, C.-K.; Tanner, P. A. Electronic spectra and crystal field analysis of Yb^{2+} in $SrCl_2$. *Phys. Rev. B.* **2008**, *77*, art. no. 085114.
45. Thompson, L. C.; Serra, O. A.; Schwartz, R. W. Emission spectra of $Cs_2NaTbCl_6$ and Cs_2NaYCl_6:Tb^{3+}. *Chem. Phys.* **1977**, *26*, 393–401.
46. Morrison, I. D. Two-photon spectroscopy of some inorganic systems. *D. Phil. Thesis*, University College, Oxford, England. 1992. page 72.
47. Ryan, J. L.; Jørgensen, C. K. Absorption spectra of lanthanide hexahalides. *J. Phys. Chem.* **1966**, *70*, 2845–2857.
48. van't Spijker, J. C.; Dorenbos, P.; van Eijk, C. W. E.; Wickleder, M. S.; Güdel, H. U.; Rodnyi, P. A. Scintillation properties of some Ce-doped chloride elpasolites. *J. Lumin.* **1997**, *72–74*, 786–788.
49. Prokofiev, A. V.; Shelykh, A. I.; Melekh, B. T. Periodicity in the band gap variation of Ln_2X_3 (X=O, S, Se) in the lanthanide series. *J. Alloys Compds.* **1996**, *242*, 41–44.